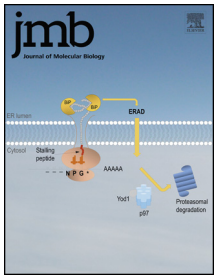

A New Mechanism for High-Affinity Uptake of C4-Dicarboxylates in Bacteria Revealed by the Structure of *Rhodopseudomonas palustris* MatC (RPA3494), a Periplasmic Binding Protein of the Tripartite Tricarboxylate Transporter (TTT) Family

Leonardo T. Rosa, Samuel R. Dix, John B. Rafferty and David J. Kelly

Department of Molecular Biology and Biotechnology, *The University of Sheffield, Firth Court, Western Bank, Sheffield, S10 2TN, UK*

Correspondence to David J. Kelly: *d.kelly@sheffield.ac.uk*
https://doi.org/10.1016/j.jmb.2018.11.016
Edited by Bert Poolman

Abstract

C4-dicarboxylates play a central role in cellular physiology as key metabolic intermediates. Under aerobic conditions, they participate in the citric acid cycle, while in anaerobic bacteria, they are important in energy-conserving fermentation and respiration processes. Ten different families of secondary transporters have been described to participate in C4-dicarboxylate movement across biological membranes, but only one of these utilizes an extracytoplasmic solute binding protein to achieve high-affinity uptake. Here, we identify the MatBAC system from the photosynthetic bacterium *Rhodopseudomonas palustris* as the first member of the tripartite tricarboxylate transport family to be involved in C4-dicarboxylate transport. Tryptophan fluorescence spectroscopy showed that MatC, the periplasmic binding protein from this system, binds to L- and D-malate with K_d values of 27 and 21 nM, respectively, the highest reported affinity to date for these C4-dicarboxylates, and to succinate (K_d = 110 nM) and fumarate (K_d = 400 nM). The 2.1-Å crystal structure of MatC with bound malate shows a high level of substrate coordination, with participation of two water molecules that bridge hydrogen bonds between the ligand proximal carboxylic group and the main chain of two conserved loops in the protein structure. The substrate coordination in MatC correlates with the binding data and explains the protein's selectivity for different substrates and respective binding affinities. Our results reveal a new function in C4-dicarboxylate transport by members of the poorly characterized tripartite tricarboxylate transport family, which are widely distributed in bacterial genomes but for which details of structure–function relationships and transport mechanisms have been lacking.

Introduction

C4-dicarboxylates play essential roles in both prokaryotic and eukaryotic central metabolism. Under aerobic conditions, succinate, fumarate and malate are key intermediates of the complete oxidative citric acid cycle that yields NADH for respiration driven proton translocation leading to ATP synthesis; succinate itself is also a direct electron donor to the quinone pool through succinate dehydrogenase [1]. Under anaerobic conditions, C4-dicarboxylates are used in a variety of fermentative or anaerobic respiratory pathways in different bacteria. In facultative anaerobic bacteria such as *Escherichia coli*, fumarate acts as an electron acceptor and is reduced to succinate (fumarate respiration), which is then excreted [1]. In many anaerobic bacteria, a proton-motive force can be generated by decarboxylation of C4-dicarboxylic acids. For example, in *Lactococcus lactis*, L-malate is decarboxylated to lactate [2], while in *Pseudomonas* sp., fumarate is converted to pyruvate [3]. Many environmental bacteria, such as those belonging to the genera *Pseudomonas, Rhodopseudomonas* and

Rhizobium, prefer to use organic acids as their main carbon source [4–6]. In the latter, the uptake of C4-dicarboxylates, especially L-malate, is linked to their ability to perform nitrogen fixation in symbiosis with different legume crops [7].

Bacteria have evolved several different transport mechanisms for C4-dicarboxylates, but none of these appear to be primary transporters (i.e., using free energy from a chemical energy source, often ATP hydrolysis). Rather, these transporters use electrochemical ion-gradients, such as the proton-motive force, Na^+ gradient or the concentration gradient of the organic acids themselves, as in the case of many antiporter systems [8]. At least 10 different secondary transporter families are currently known to be involved in C4-dicarboxylate transport. By far, the best studied systems are the DctA homologs, belonging to the dicarboxylate/amino acid:cation symporter (DAACS) family (TC 2.A.23). DctA homologs are present in most of the bacterial kingdom but are not found in strictly anaerobic bacteria. They have been extensively characterized in *E. coli* and also in *Rhizobium* species, where they are essential for L-malate transport that fuels symbiotic nitrogen fixation [7,9]. DctA performs most of the C4-dicarboxylate uptake in bacteria under aerobic conditions and neutral pH, where these molecules are largely in di-anionic form and are transported in an electrogenic fashion. DAACS members can have a broad substrate range and K_m values varying from 2 to 30 μM [1,9,10]. While in most bacteria transport by the DAACS family is dependent on an H^+ gradient, in some bacteria such as *Corynebacterium glutamicum*, an Na^+ gradient energizes transport [11]. In alder root cells, the C4-dicarboxylates are provided to the bacteria through export by the AgDCAT1 protein, a member of the proton-dependent oligopeptide transporter (POT/PTR) family (TC 2.A.17) [12].

In aerobic but acidic environments (pH 5–6), transporters from the sulfate permease (SulP) family (TC 2.A.53) can efficiently catalyze C4-dicarboxylate uptake. Conserved from bacteria to humans, these transporters move the substrates in their mono-anionic form, with H^+ as the coupling ion. The DauA protein, from *E. coli*, is the best-characterized protein from this family [1]. Under anaerobic conditions, on the other hand, proteins from the DcuAB family (TC 2.A.13), such as DcuA and DcuB from *E. coli*, catalyze the electroneutral antiport of fumarate and succinate to allow for fumarate respiration, but are also capable of electrogenic uptake and efflux and allow for some substrate flexibility [10]. The substrate K_m values for transport in this family range from 50 to 100 μM [1,13]. Proteins from the DcuC family (TC 2.A.61) were found to have very similar function to the DcuAB family and similar affinities, but are mostly characterized as succinate exporters under conditions of hexose fermentation [1,10].

Also conserved from bacteria to humans, proteins belonging to the divalent anion:sodium symporter (DASS) family (TC 2.A.47) are involved in the uptake of citrate and dicarboxylic acids [8]. Previously characterized as citrate transporters in chloroplasts and mitochondria, members of this family were shown to be the major uptake system for C4-dicarboxylates in some free-living bacteria, such as the DccT protein from *C. glutamicum* [14,15]. The best-studied systems are the C4-dicarboxylate:Na^+ symporter VcINDY (*Vibrio cholerae*) [16,17] and the TtdT tartrate-succinate antiporter from *E. coli* [1]. Members of this family can have a very wide range of substrate affinities, with K_m values from 2 to 300 μM for different C4-dicarboxylates [17].

Other protein families associated with the transport of C4-dicarboxylates have either very low substrate affinity and thus reduced physiological relevance, or are associated with very specific processes and not represented in many bacteria. SatP, from *E. coli*, is a member of the acetate uptake transporter (AceTr) family (TC 2.A.96) and catalyzes the symport of either succinate or acetate with H^+, under acidic conditions, with a characterized K_m of 1.8 mM [1]. In some bacteria, L-malate: H^+ symport is performed by members of the 2HCT family (TC 2.A.24), such as the MaeN (*Bacillus subtillis*) and MaeP (*Streptococcus bovis*) symporters [18]. In addition, the MleP malate/lactate electroneutral antiporter is crucial for malolactic fermentation in *L. lactis*, and this antiporter activity is also observed in *B. subtillis* as the product of MleN activity, which belongs to the NhaC family (TC 2.A.35) [18].

The transport of substrates from very low external concentrations, as found in many natural environments, requires high-affinity, solute binding protein (SBP)-dependent transporters, involving extracytoplasmic (periplasmic in gram-negative bacteria) SBPs, which tightly bind their ligands and deliver them to their respective membrane counterparts [19]. They are of three different families: the primary ATP-binding cassette family (ABC; TC 3.A.1), not found to date to transport C4-dicarboxylic acids, and two secondary systems, the tripartite ATP-independent periplasmic (TRAP) transporters (TC 2.A.56) and tripartite tricarboxylate transporters (TTT; TC 2.A.80) [19]. Although the TRAP and TTT systems show no sequence similarity, they both consist of a large [12-transmembrane (TM) helix] and small (4-TM helix) membrane protein in addition to the periplasmic SBP that endows these systems with high substrate affinity [19]. The prototype TRAP system, DctPQM of *Rhodobacter capsulatus*, was the first periplasmic binding protein-dependent C4-dicarboxylate uptake system discovered, with DctP binding to its substrates with K_d values ranging from 50 nM for L-malate to 250 nM for fumarate, and 6.3 μM for D-malate [20]. DctPQM homologs have subsequently been described in many bacteria, but the range of substrates

taken up by TRAP systems has expanded considerably beyond C4-dicarboxylates [21], as has knowledge regarding the biochemical properties of this family, which are energized by an electrochemical sodium-ion gradient [22].

The TTT family, however, remain poorly characterized, and their energy coupling mechanisms are unclear [19]. Although the prototype system for this family, the citrate transporter TctCAB from *Salmonella typhimurium,* was first characterized 40 years ago [23], very few substrates for this family are currently known, but evidence is emerging that these are not restricted to tricarboxylates, as reviewed by Rosa *et al*. [19]. Among the sequenced genomes of α and β-proteobacteria, genes for the SBP components of this family can be hugely overrepresented, reaching 434 genes in *Rhodoplanes* sp. Z2-YC6860, which accounts for 6% of all genes in its genome [24]. This very high representation of orphan SBPs suggests that their physiological relevance has been underestimated. In a previous study, we characterized AdpC, a TTT SBP from the purple non-sulfur bacterium *R. palustris*, that binds dicarboxylates ranging from 6 to 9 carbons in chain length, particularly adipate and pimelate [25]. *R. palustris* contains operons for two complete TTT systems plus five orphan proteins from the TTT SBP family, including AdpC. This study presents the biochemical and structural characterization of MatC, the SBP component of one of the complete systems (MatBAC). We show that L- and D-malate bind to MatC with nanomolar K_d values, the highest affinity described to date for a C4-dicarboxylate transport protein, and with somewhat lower affinity to fumarate and succinate. The high-resolution crystal structure of the malate bound MatC shows multiple substrate coordination contacts, which successfully explains the high affinity and substrate selectivity of MatC. The discovery of a C4-dicarboxylate transporter in the TTT family expands the known mechanisms by which bacteria utilize these substrates and paves the way for future studies of the transport and energy-coupling mechanisms of TTT systems.

Results

Identification, purification and oligomeric state of MatC

Two complete (i.e., all three genes operonically encoded) TTT systems from *R. palustris* CGA0009 were identified using BLAST analysis, as described by Rosa *et al*. [19]. TttBAC1 (of unknown function) is encoded by genes *rpa2321–2319* and TttBAC2, the focus of this study, is encoded by genes *rpa3496–3494* (Fig. 1a). Given our characterization of TttC2 as a malate binding protein (see below), we suggest TttBAC2 be designated as MatBAC (*m*alic *a*cid *t*ransporter; Fig. 1a) and will use this designation henceforth. The *rpa3494* gene encoding MatC, the SBP component of the MatBAC system, was cloned, overexpressed as a C-terminally hexa-histidine (His_{6x}) tagged protein and purified by nickel affinity chromatography (Fig. 1b). MatC is composed of 335-amino-acid residues, of which 307 are present in the 32.6-kDa mature protein, after signal peptide cleavage. After cloning in pET21a, the mature 307-aa protein fused with the tag resulted in a 34-kDa protein. Size exclusion chromatography (Fig. 1c) showed that MatC was eluted at 16.22 mL of buffer, which in the calibration curve provided in Fig. 1d would be equivalent to 39 kDa, suggesting that the protein is a monomer.

Differential scanning fluorescence assays reveal MatC binds to C4-dicarboxylates

MatC was screened against a library of 84 compounds comprising organic acids, amino acids, vitamins, aromatic compounds, sugars and nitrogenated compounds, using a differential scanning fluorescence assay, as described by Rosa *et al*. [25], which exploits the enhancement of SYPRO orange fluorescence as it binds to interior hydrophobic regions of the protein during thermal denaturation. Of the compounds screened, large increases in the melting temperature of MatC were observed in the presence of the C4-dicarboxylates DL-malate (9 °C), succinate (7 °C) and fumarate (6 °C), respectively, as shown in Fig. 2a, indicative of ligand-dependent thermal stabilization. However, no stabilization was observed with other C4-carboxylates, such as tartrate, oxaloacetate or mesaconate, or with acetoacetate, aspartate, crotonate or butyrate (Fig. 2b, c). The absence of a thermal shift in the presence of butyrate suggests that both carboxylic groups are essential for substrate coordination. Furthermore, although a hydroxyl group on the C2 position of the screened compound seems to improve protein stabilization, the substitution of this group for a carbonyl or methyl group in oxaloacetate and mesaconate, respectively, does not result in stabilization, nor does the addition of another hydroxyl group on carbon 3, as shown in the presence of tartrate. The absence of a thermal shift in the presence of malonate and glutarate suggests also that MatC strictly binds substrates with a chain length of four carbons. Notably, MatC did not show thermal stabilization upon the addition of citrate, found in several organisms to be a common ligand for the TTT family [26–29].

Malate binds to MatC with nanomolar affinity

A pronounced quench was observed in protein intrinsic tryptophan fluorescence when MatC (0.2 μM) was incubated in the presence of 1 mM DL-malate,

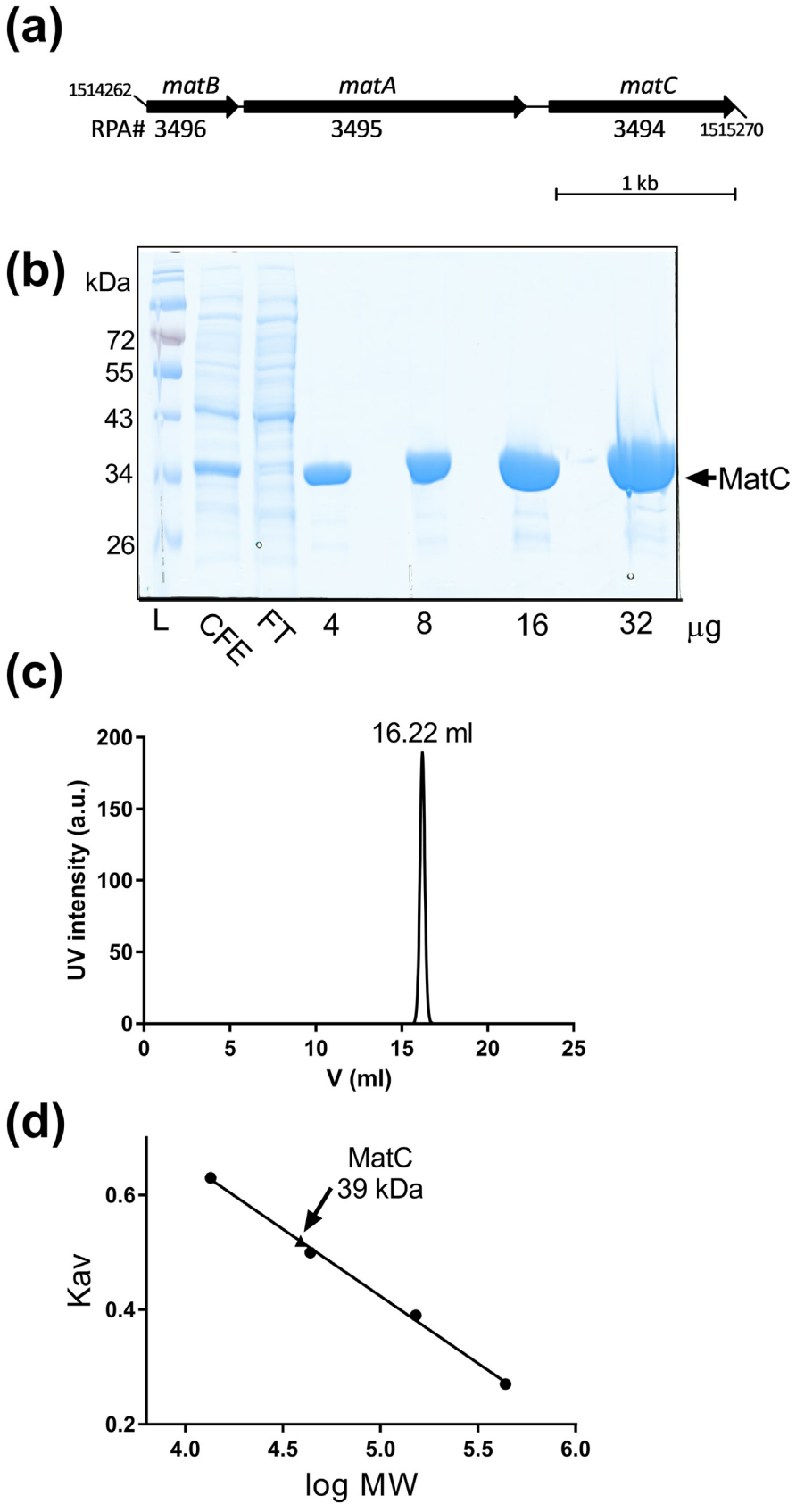

Fig. 1 (*legend on next page*)

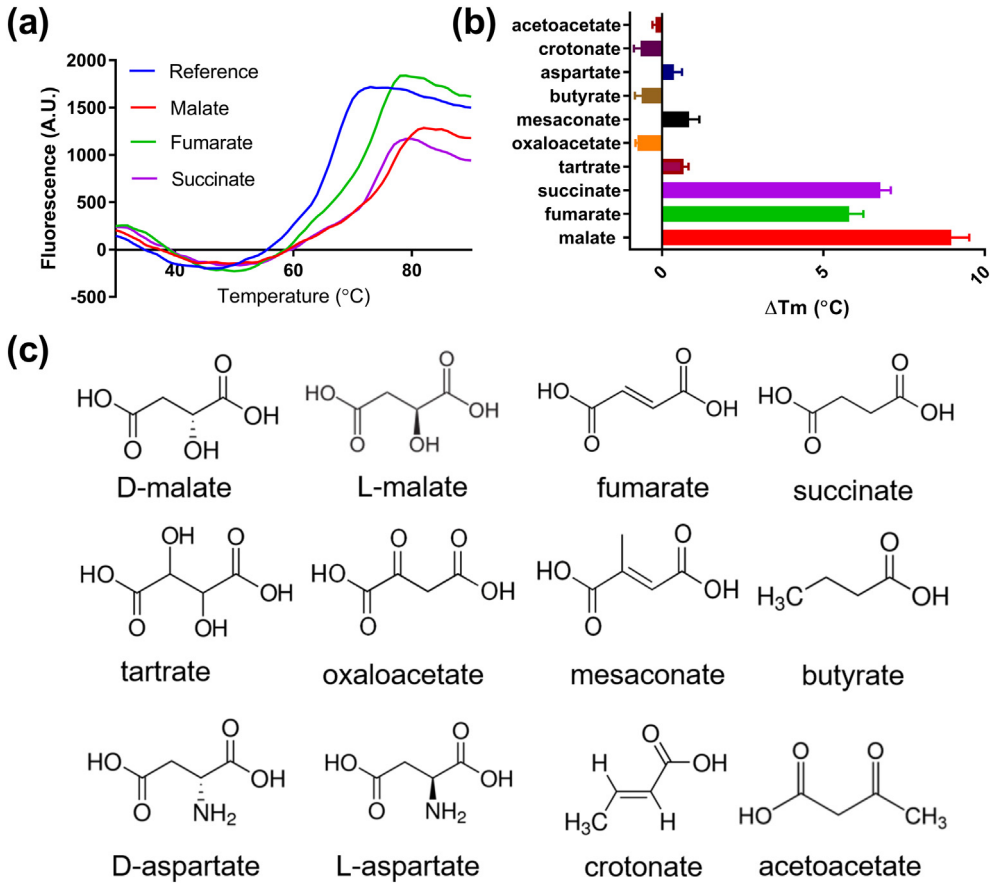

Fig. 2. Differential scanning fluorescence (DSF) assay of MatC. (a) Thermal shift profile of MatC alone (reference trace) and in the presence of DL-malate (red trace), succinate (purple trace) or fumarate (green trace). Assays were performed with 5 μM protein in TF Buffer [Tris–HCl 50 mM (pH 7.4), NaCl 0.1 M], 1× SYPRO orange dye concentration and 60 μM ligands. (b) MatC thermal stabilization in the presence of selected ligands. Each bar shows the mean and standard deviation of the thermal shift from three independent assays compared to no ligand. (c) Structure of the ligands used for DSF assay.

fumarate or succinate, with reductions of ~21%, ~13% and ~9% respectively, in the fluorescence emission at 335 nm compared to the control (Fig. 3a). Confirming the results from the differential scanning fluorescence assay, no quench was observed in the presence of tartrate, oxaloacetate, mesaconate, butyrate, acetoacetate, aspartate, crotonate or citrate.

In order to determine binding affinity, ligand titrations of the tryptophan fluorescence change were performed, as described in Materials and Methods. MatC was found to bind very tightly to both isomeric forms of malate, with a K_d value of 21 ± 2 nM for D-malate and 27 ± 2 nM for L-malate, the highest affinity described for any C4-dicarboxylate transporter, and apparently

Fig. 1. Purification of the MatC recombinant protein. (a) Genomic localization and organization of the *matBAC* operon. (b) Coomassie blue-stained SDS-PAGE gel of MatC purification. Samples were loaded in the following order: molecular weight ladder (L); cell-free-extract obtained after induction showing the MatC band at ~34 kDa; flow through before initiating the imidazole elution (FT), showing absence of the MatC band. The remaining lanes show increasing amounts (4, 8, 16 and 32 μg of protein per lane, as indicated) of pure MatC obtained after the nickel affinity and size exclusion chromatography (see Materials and Methods). (c) Size exclusion chromatography of MatC. The protein was run in 50 mM Tris–HCl (pH 8.0) plus 0.5 M NaCl. Elution of protein was observed after 16.22 mL of buffer, which in the corresponding calibration curve (d) would be equivalent to 39 kDa, near the estimated size for an MatC monomer, of 34 kDa. Calibration curve was generated using ferritin (440 kDa), aldolase (150 kDa), ovalbumin (44 kDa) and ribonuclease (13.5 kDa), and K_{av} was calculated using the standard formula K_{av} = (Ve – Vo)/(Vt – Vo), where Ve is elution volume, Vo is column void volume and Vt is total column volume.

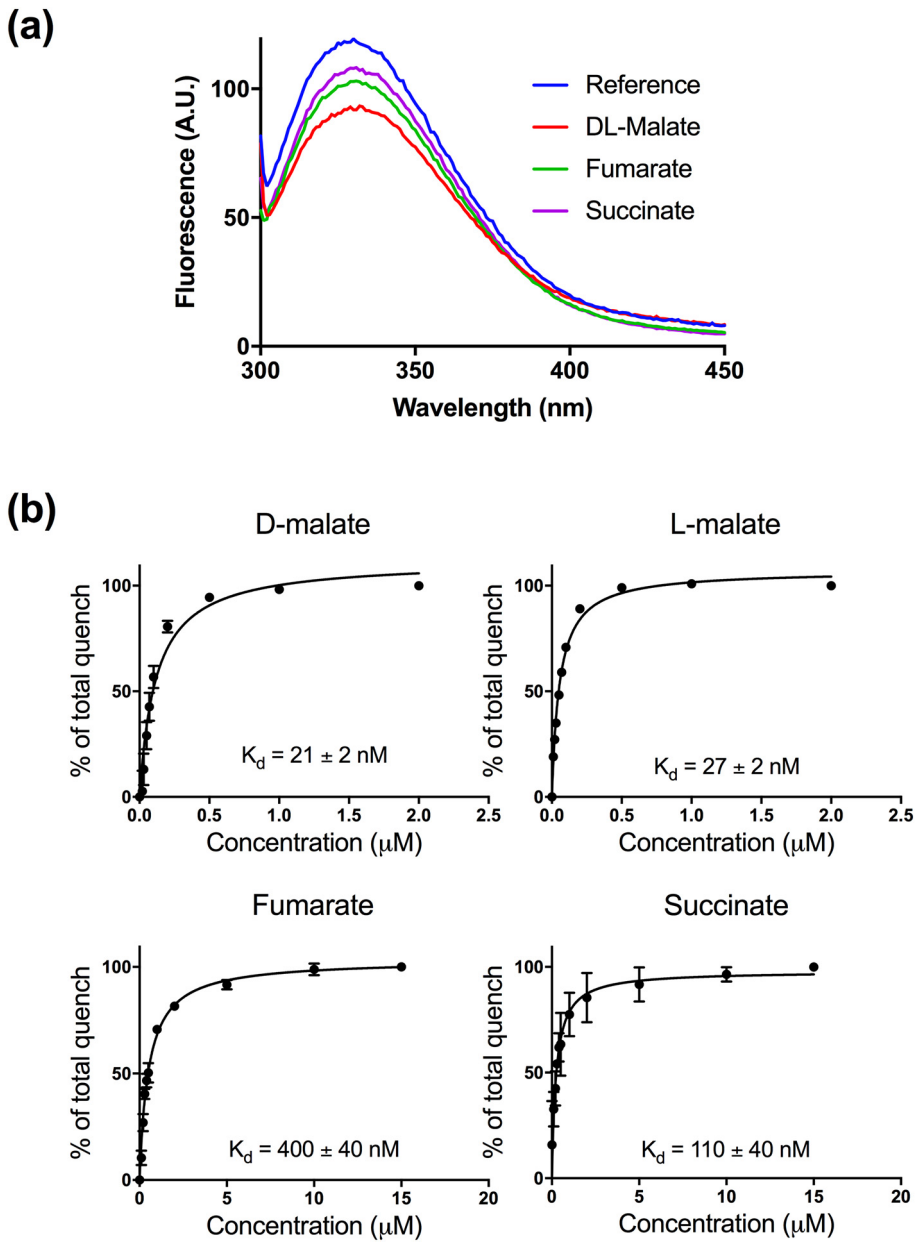

Fig. 3. Evidence for binding of C4-dicarboxylates to MatC by changes in intrinsic tryptophan fluorescence. (a) Changes in the emission spectrum of MatC (0.2 μM) in the presence of different C4-dicarboxylates (1 mM). Excitation was at 280 nm and the emission scanned from 300 to 450 nm. (b) Titration of MatC fluorescence emission with C4-dicarboxylates. Protein was assayed at 0.2 μM concentration in 3 mL of TF buffer [Tris–HCl 50 mM (pH 7.4), NaCl 0.1 M] at 30 °C with continuous stirring. Titrations were made in triplicate; data points are means with error bars showing standard deviation (in many cases too small to be seen). Excitation and emission wavelengths were 280 and 335 nm, respectively. K_d calculations were performed using the quadratic equation for tight binding as previously described [47].

not distinguishing between the two enantiomeric forms as previously described for the other transport families (Fig. 3b) [1,9,10]. Lower affinities were observed for succinate and fumarate, with K_d values of 110 ± 40 and 400 ± 40 nM, respectively (Fig. 3b). These results suggest that the hydroxyl group on carbon 2 (Fig. 2c) must play an important role in substrate coordination in the protein-binding pocket. When size exclusion chromatography was repeated in the presence of 1 mM DL-malate, the protein also eluted as a monomer, suggesting that ligand binding does not cause oligomerization, as has been observed for some binding-proteins of certain TRAP transporters [30–32].

matC gene expression is increased in the presence of C4-dicarboxylates but the phenotype of a *matBA* deletion mutant indicates transporter redundancy

In order to investigate if *matC* gene expression is responsive to the presence of C4-dicarboxylates as growth substrates for *R. palustris*, reverse transcription–polymerase chain reaction (RT-PCR) was used to measure differences in gene expression under photoheterotrophic growth conditions with 10 mM DL-malate, fumarate or succinate as sole carbon sources in minimal media. The results (Fig. 4a) show increased transcription levels at mid-log phase relative to growth with the C3-monocarboxylate control substrate pyruvate. Mean increases in *matC* expression of 3.3-, 2.1- and 1.6-fold compared to pyruvate (set at 1-fold) were observed when malate, succinate or fumarate, respectively, were used as sole carbon source. These results support a physiological role for MatC and thus the MatBAC system during growth on C4-dicarboxylates. However, bacteria often express multiple transporters for the same substrate, and so to determine the relative contribution of the MatBAC system to growth on C4-dicarboxylates, we constructed a chromosomal deletion strain lacking the membrane components from the operons of both of the complete TTT systems in *R. palustris*, that is, a *tttBA1/matBA* strain (Supplementary Fig. 1). The double mutant was made in order to rule out the possibility that one TTT SBP (i.e., MatC) might be able to interact with more than one TM component, as suggested previously in view of the common over-representation of the SBP genes compared to the membrane protein genes for TTT systems [19]. As shown in Fig. 4b, no difference was observed in growth between the wild-type and the double-mutant strain, when using 10 mM DL-malate, succinate or fumarate as the sole carbon source in comparison to the non-C4-dicarboxylate control substrate phenylvalerate (on which *R. palustris* grows well). Taken together, the data suggest that MatBAC is not essential for the uptake of C4-dicarboxylates under these conditions and that other transporters contribute (see Discussion).

The 2.1-Å resolution structure of MatC

MatC was successfully crystallized in the presence of a 1 mM racemic mixture of D- and L-malate. A protein crystal structure was obtained at 2.1-Å resolution with substrate coordinated in the binding pocket, as shown in Figs. 5a and 6a and Supplementary Fig. 2. The data suffered from some anisotropy, and completeness was low at the resolution limit (see Materials and Methods) such that the electron density more closely resembled that of a 2.4-Å map. At this resolution, it was not possible to distinguish with confidence between the D- and L-forms of the ligand. The model was refined with a half occupancy of D- and L-forms of the ligand to reflect the observed poor discrimination seen in the binding studies, and statistics provided in Table 1 are presented for the racemic mixture. Refinement using D- and L-malate separately produced essentially identical values. Three copies of MatC were present in the asymmetric unit, and RMSD values between the three, based on their alpha carbon positions, ranged from 0.27 to 0.38 Å. The following structural descriptions will refer to chain A of the coordinate file. MatC is a monomer comprising of 307 aa in the mature form (without the signal sequence) and 318 in our His-tagged recombinant construct, where residues 13 to 306 are defined in the 2.1-Å electron density map. The protein is composed of nine α-helices, nine β-strands and three 3_{10} helices (Fig. 5b). The secondary structure is organized in two globular domains separated by a hinge, formed by β4 and β9, in a "venus fly-trap"-like architecture characteristic of periplasmic binding proteins, revealing MatC as a type II binding protein according to the classification of Fukami-Kobayashi *et al*. [33] and cluster E-II according to the classification proposed by Scheepers *et al*. [34]. Each domain is composed of a β-sheet surrounded by α-helices. Domain 1 comprises residues 1–110 and 237–312, while domain two comprises residues 111–236. In domain 1, the architecture of the sheet is β2–β1–β3–β9–β4, and in domain 2, it is β6–β5–β7–β4–β8. Although the structure shows two cysteines, Cys190 and Cys155, adjacent in space, their sulfydryl groups are not directed toward each other and no electron density suggesting a disulfide bond is observed, in contrast to those described for the TTT SBPs BugD, BugE and Bug27 from *Bordetella pertussis* [29,35,36]. However, *in vivo* MatC is predicted to be located in the periplasm, which might suggest that under the natural periplasmic oxidative conditions, this disulfide bond could be formed by the Dsb system.

D-Malate coordination in MatC crystal structure

Figure 6a shows a LigPlot representation of the malate molecule coordinated in the protein binding pocket. For clarity, only the D-malate is shown, but the alignment of the two forms is such that the conclusions drawn about binding interactions are the same. In agreement with previously described structures for members of the TTT family [29], the ligand proximal carboxylic group is coordinated by two spatially conserved water molecules, which form hydrogen bonded bridges between the ligand and a "pincer-like" structure composed by two β-loops, between β1 and α1 and β6 and α5 (in MatC), respectively. These hydrogen bonds, as described for AdpC [25], are mostly made with the main chain of aliphatic residues, rather than side chains. In the

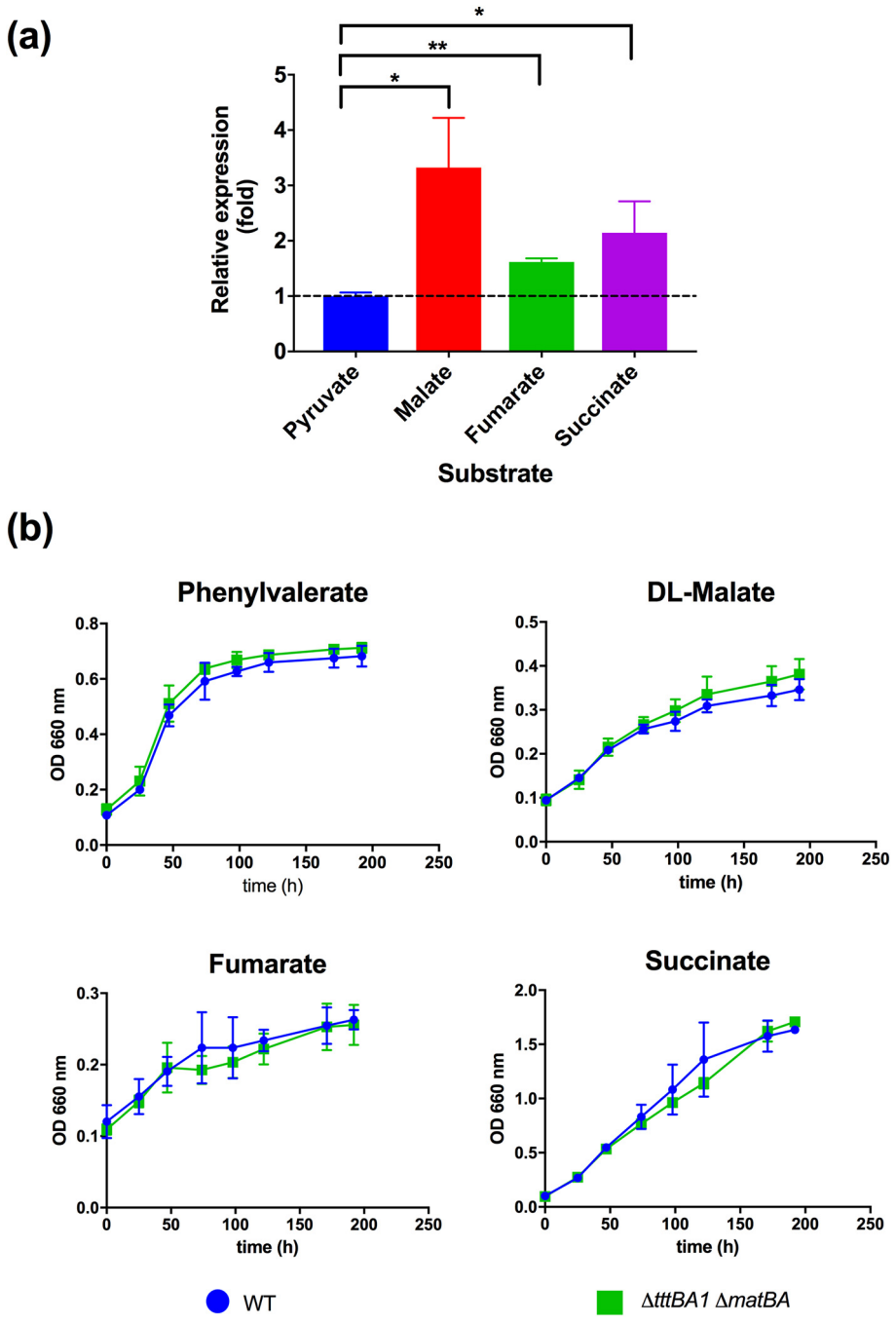

Fig. 4. (a) RT-PCR analysis of *matC* expression after growth with C4-dicarboxylates or pyruvate. The fold-changes compared to pyruvate (dotted line, set at 1-fold) are shown as means and standard deviation of three biological replicates after growing cells with 10 mM of substrate. Statistics were performed with Student's *t*-test, where * $P < 0.05$, * $P < 0.01$. (b) Growth experiments comparing *R. palustris* wild-type and a marker-free knockout mutant lacking the TttBA1 and MatBA TM proteins. Growth was performed photoheterotrophically in the presence of 10 mM substrates in biological triplicates, and absorbance was measured at 660 nm. Error bars represent standard deviation from the mean.

MatC structure, both oxygens 4 and 5, in the proximal carboxylic group of the malate molecule, alternately make bridging contacts via a water molecule with the main-chain carbonyl oxygen of Ala25 and nitrogen of Asp31. Oxygen 4 is further coordinated by another water molecule, which

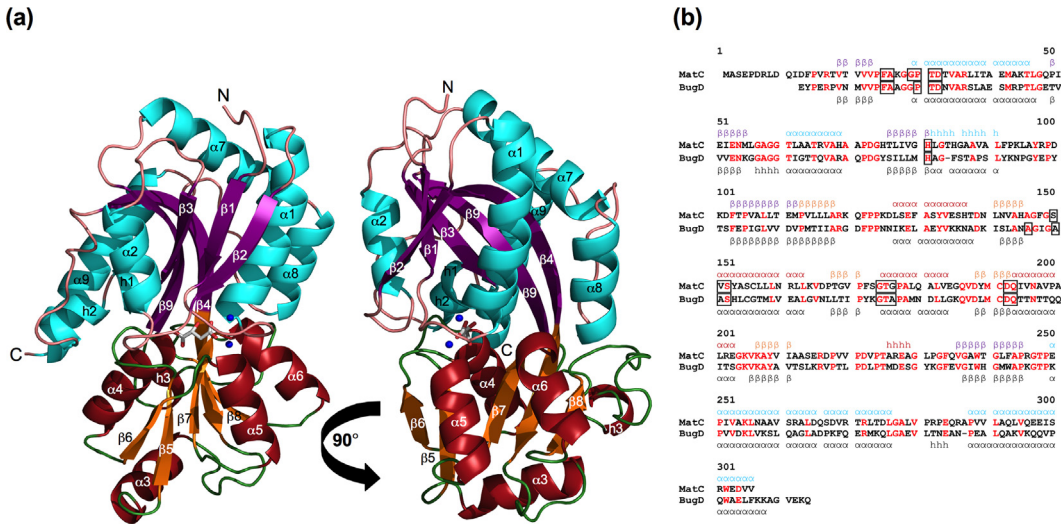

Fig. 5. Structural features of MatC. (a) Overall structure of D-malate-bound MatC. The protein is folded in a typical Venus-flytrap-like arrangement for periplasmic binding proteins, with a cleft where the substrate is coordinated, separating two globular domains composed of five stranded β-sheets surrounded by α-helices (the helices and strands for the first domain are shown in cyan and magenta and for the second domain in red and orange). The two domains are connected by a hinge formed by strands β4, which is part of both β-sheets, and β9, characterizing this protein as a member of Cluster E-II for binding protein classification [34]. Two well-conserved β-loops, between β1 and α1 and β6 and α5, form a "pincer-like" structure, which coordinate the ligand proximal carboxylic group via bridging by two conserved water molecules (blue dots in the center of the structure). (b) Protein sequence alignment between MatC and BugD. Residues highlighted in red are identical in both proteins. Boxed residues are involved in ligand coordination. Secondary structure arrangement is shown adjacent to the sequences, with the same colors as used in panel a for MatC. α, α-helix; β, β-sheet; h, 3_{10} short helix.

interacts with the main-chain nitrogen of Gly175 and carbonyl oxygen of Ala25 (Fig. 6a). In addition to water coordination, oxygen 4 on the malate has a hydrogen bond with the main-chain amino nitrogen of Thr174, and oxygen 5 with both the main-chain nitrogen and the side-chain hydroxyl of Thr30. Most of these residues are conserved among AdpC, BugD and BugE, maintaining the described conservation and relevance of this "pincer-like" domain among the TTT family [35]. A third water molecule is involved in coordination of oxygen 2 in the distal carboxylic group, as seen in all previous structures. This water bridges hydrogen bonds between oxygen 2 and the nitrogens from the main-chain and side-chain carboxamide of Gln192, in addition to the side-chain carboxylic group of Asp191. Oxygen 2 makes further direct hydrogen bonds with the main-chain nitrogen and side-chain oxygen of Ser151, where oxygen 1 contacts the main-chain nitrogen of Val150 and the imidazole nitrogen of His80. The carbon 2 hydroxyl group in malate is coordinated also by a hydrogen bond with the side-chain oxygen in Thr30 and with the side chain of Gln192, irrespective of whether it is modeled and refined in the D- or L-forms. In addition, a few other residues are involved also in hydrophobic interactions. These are as follows: Phe24, noted previously as a hydrophobic platform that interacts with the carbon backbone of the ligand in all investigated TTT transporter SBPs [25]; Gly28; Pro29; Ser149; and Gly173.

Comparison of ligand coordination between MatC and BugD

There is a striking 60% sequence similarity and 39% identity between MatC and BugD, a TTT SBP from the beta-proteobacterium *B. pertussis* [35] (Fig. 6b), which is also reflected in the similarity of their ligands. The structure of BugD was reported with what was assumed to be a bound L-aspartate molecule, liganded fortuitously and retained during the purification and crystallization process [35]. Aspartate and malate have similar structures and potential binding interactions that are difficult to distinguish in electron density maps, with simply an amine in aspartate replacing the hydroxyl group on carbon 2 in malate. The substrate coordination overlaps almost entirely in both the MatC and BugD protein structures, as shown in Fig. 3b (blue and magenta dots for MatC and BugD, respectively). Only two residues involved in hydrogen bond coordination are not conserved: Val150 and Gly175 (in MatC), which are both substituted in BugD for alanine (Fig. 6b) without any effect upon the coordination as this involves only main-chain atoms for these residues. There is no evidence for binding of aspartate

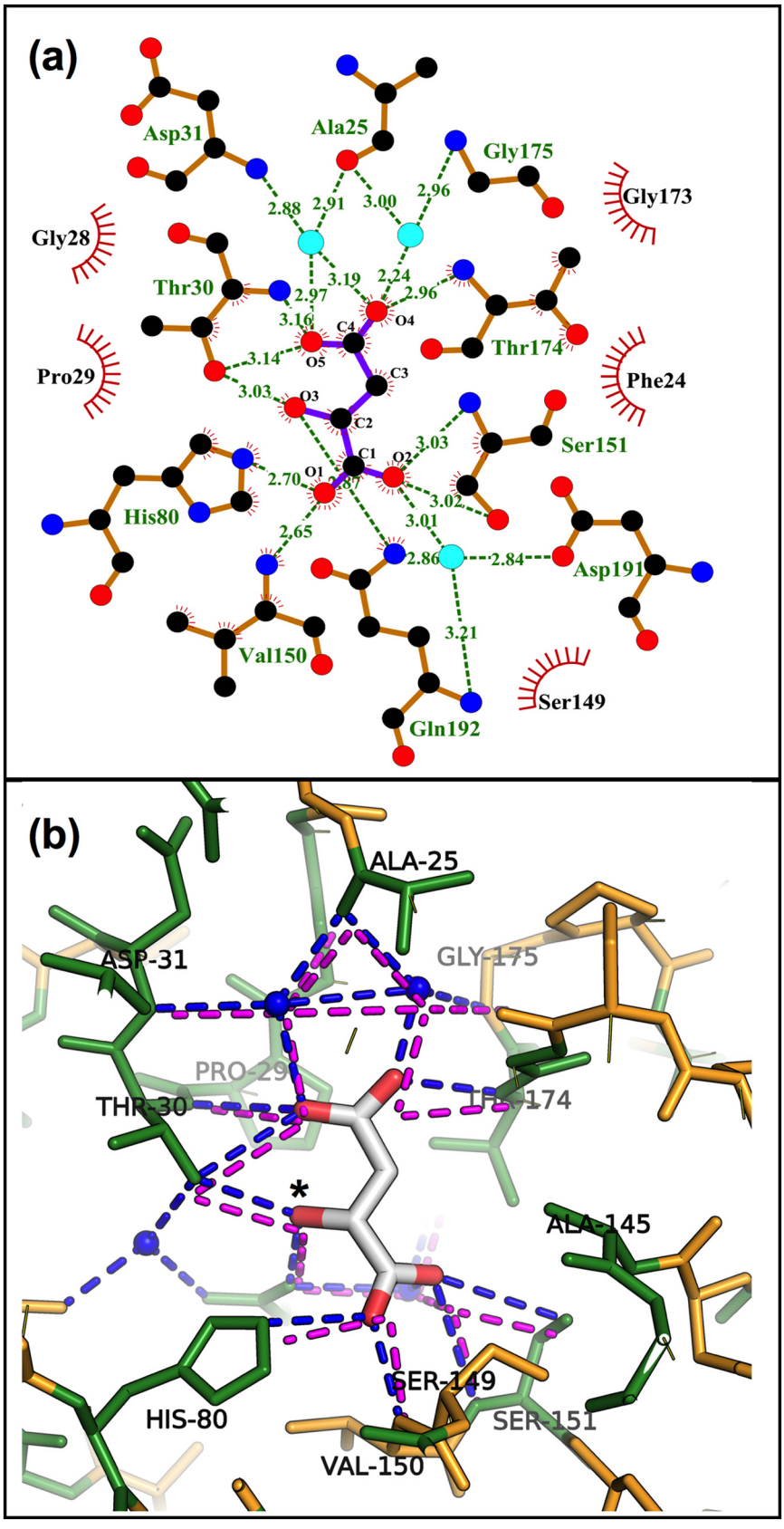

Fig. 6 (*legend on next page*)

Table 1. Data processing and model refinement statistics

	MatC 6HKE
Data collection	
Wavelength (Å)	0.97949
Resolution range (Å)	63.54–2.11 (2.17–2.11)
Space group	$P2_12_12_1$
Cell dimensions	
a, *b*, *c* (Å)	80.8, 205.8, 47.6
α, *β*, *γ* (°)	90, 90, 90
Total reflections	76,223 (4478)
Unique reflections	41,492 (2471)
Multiplicity	1.8 (1.8)
Completeness (%)	88.9 (65.3)
Mean *I*/σ*I*	12.4 (1.6)
R_{merge}	0.046 (0.591)
Refinement	
R_{work}/R_{free}	0.191/0.248
No. atoms	
Protein	6603
Ligand	54
Water	113
B-factor (Å^2)	
Protein	31.9
Ligand	26.3
Water	27.0
RMSD from target	
Bond length (Å)	0.007
Bond angle (°)	1.547
Ramachandran plot analysis (%)	
Total favored	98
Total allowed	100

Outer-shell data in parenthesis.

by MatC, as tested through differential scanning fluorescence and tryptophan fluorescence assays.

Discussion

In this study, we identified the periplasmic SBP MatC as part of the MatBAC system, one of the two complete TTT family systems in *R. palustris* [19]. Upon screening of MatC against a library of compounds using differential scanning fluorescence, we observed protein thermal stabilization in the presence of the C4-dicarboxylates malate, succinate and fumarate. The screening showed MatC to have a high ligand specificity, only allowing C4 dicarboxylate binding with restricted substitution at C2. This degree of specificity is present in some of the TTT SBPs characterized so far, such as the terephthalate binding protein ThpC [37] and the sulfolactate binding protein SlcH [38], but is not seen in others such as AdpC, which binds dicarboxylates from six to nine carbons in length [25], or in Bug27, which was reported to bind nicotinate, nicotinamide, benzoate and citrate [29]. MatC showed no indication of binding to citrate, the prototype ligand that gave rise to the family name and binding of which has been characterized for TTT systems in many organisms such as *S. typhimurium*, *B. pertussis, C. glutamicum* and *L. lactis* [23,27,29,39].

Titration of MatC with ligands, using intrinsic tryptophan fluorescence analysis, revealed a binding affinity of ~20 nM for both the D- and L-isomers of malate. This affinity is 2 orders of magnitude higher than the highest affinity described previously for DctA homologs and for members of the DAAS family [9,16], emphasizing the effectiveness of SBP-mediated transport at low environmental ligand concentrations. In addition, the K_d values for MatC are slightly less than half of the 50 nM L-malate affinity described for the *R. capsulatus* DctP SBP, belonging to the TRAP transporter family [20], thus making MatBAC from *R. palustris*, the uptake system with the highest reported affinity for C4-dicarboxylates, to the best of our knowledge. MatC also showed higher affinity than the micromolar affinity found for other binding proteins in the TTT family [23,25,26,29]. Although Sweet *et al*. [26] demonstrated that succinate and malate were capable of displacing citrate binding in *S. typhimurium* TctC when present in millimolar concentrations, this is the first high-affinity, dedicated TTT system described to bind C4-dicarboxylates.

The RT-PCR analysis of *matC* suggests an increase in expression during growth in the presence of C4-dicarboxylates. However, deletion of both TTT TM systems did not affect the growth phenotype of *R. palustris* in the presence of 10 mM of the C4-dicarboxylate substrates. C4-dicarboxylic acids are

Fig. 6. Malate co-ordination in the MatC binding pocket. (a) Schematic of the malate binding interactions to MatC. Traces represent hydrogen bond interactions with the respective distances, and red dashes represent hydrophobic interactions. Coordination of the α-carboxylic group by two water molecules is a conserved feature among the TTT family, bridging hydrogen bonds with the main-chain residues. Figure produced using LigPlot+ [56]. (b) Comparison between the binding interactions for malate coordination in MatC and proposed aspartate coordination in BugD. A malate molecule is shown in the binding pocket on MatC, with its interactions and the conserved water molecules shown in blue. The identical distribution of interactions seen for the proposed aspartate binding to BugD is shown in magenta. The side chains of residues in the binding pocket conserved between MatC and BugD are highlighted in green. Dashed lines represent hydrogen bonds, and blue spheres represent the water molecules. The difference between the substrate molecules is the replacement of the hydroxyl group (marked with *) at carbon 2 in malate by an amino group in aspartate. The high structural similarity strongly suggests that the ligand bound by *B. pertussis* BugD from the cytoplasm of its *E. coli* host during its production may be malate rather than aspartate.

the most favored and physiologically relevant carbon sources for soil phototrophic bacteria such as *R. palustris*, which are poorly capable of metabolizing sugars [4,40]. Thus, it is expected that this bacterium would have evolved to optimize the uptake of C4-dicarboxylates. In *R. palustris* CGA009, 16% of the genome encodes for transport-related proteins [4], and it is thought to contain redundant transport systems for many substrates [41]. Indeed, the genomic analysis of Larimer *et al*. [4] describes one DauA homolog (RPA4326), two DctA homologs (RPA0552 and RPA2448) and eight different TRAP transporters in strain CGA009, revealing a high potential for redundant uptake of C4-dicarboxylates under different environmental conditions. Although DctA and DauA proteins are conventionally associated with uptake under aerobic conditions, their activity does not require oxygen, and it might be that these homologs are regulated to respond to different environmental conditions in *R. palustris*. Furthermore, as MatBAC is a transporter with a high-affinity substrate binding-protein, it is likely that it will have more physiological relevance under low substrate concentrations, where a higher affinity and higher specificity would be needed. This is a challenging condition to access using batch culture growth experiments.

A structure of MatC was obtained with malate coordinated in the binding pocket, showing a typical "Venus fly-trap"-like conformation, with two globular domains characteristic of many types of periplasmic binding proteins. Coordination of malate is mediated by a "pincer-like" structure formed by two β-loops between β1 and α1 and β6 and α5, which coordinate the proximal carboxylate group in the substrate through hydrogen bonds bridged by two spatially conserved water molecules. This appears to be a signature motif among the TTT family, suggesting that as more substrates are identified, carboxylate functional groups will prove to be key to the initial interaction with the SBP [19]. Similarly to AdpC [25], no positively charged residues are present in the binding pocket to counteract the negative charges of the substrate carboxylic groups. In addition to the dissipation provided by the water molecules bridging hydrogen bonds with these groups, the charges might be neutralized in part by the helix dipoles from the N-termini of α1 and α5 at the proximal carboxylic group and α4 at the distal carboxylic group [42].

The additional hydrogen bonding potential provided by the hydroxyl group at the carbon 2 of malate is likely to be responsible for the higher affinity of MatC for this substrate, when compared to succinate and fumarate, both with no substitution at carbon 2. Moreover, it is possible to conjecture why the related small carboxylic acids mesaconate, butyrate, tartarate and oxaloacetate did not show any indication of binding in the fluorescence quenching and differential scanning fluorescence experiments. Mesaconate has a methyl group at the carbon 2 position in place of the hydroxyl found in malate which would not form favorable bonding interactions. For butyrate, the absence of a second carboxyl group would remove favorable coordination effects and decrease the affinity. This reinforces the hypothesis suggested by Rosa *et al*. [25] that not only one but two carboxylic groups might be generally preferred for binding in this family. The only exception to this known currently is the binding of nicotinate, nicotinamide and benzoate by Bug27 [29]. Tartrate has an additional hydroxyl group at carbon 3, which would be likely to cause steric clashes in the binding pocket around the side chains of Thr174 and Ala145. In oxaloacetate, there is an exchange of a keto oxygen for the hydroxyl at carbon 2 in malate. Clearly, the keto oxygen is unable to donate a hydrogen bond to Thr30, but it can still accept hydrogen bonds and there is little indication that problems would arise from a steric clash with the residues in the binding pocket. This is a remarkable apparent discrimination between these closely related dicarboxylic acid molecules.

A surprising similarity in substrate coordination was observed between MatC and *B. pertussis* L-aspartate binding protein BugD [35], where most of the residues and hydrogen bonds involved in coordination are conserved. Aspartate differs from malate only in the substitution of the carbon 2 hydroxyl group for an amino group. However, MatC showed no indication of binding to aspartate either by DFS or tryptophan fluorescence assay. While the neutral C2 hydroxyl group of malate provides further potential for hydrogen bonding with the main structure, the binding of an aspartate molecule in the binding pocket would place a positively charged amino group in that position. Given their structural similarity, malate and aspartate would be indistinguishable in an electron density map, except at very high resolution. With these considerations, and the fact that the identification of aspartate binding by BugD was derived from the fortuitous co-purification of a ligand with the protein, which was not confirmed by biochemical analysis [35], it is a possibility that the electron density ascribed to L-aspartate in the BugD structure actually arises from L-malate.

In summary, we have identified the first system from the poorly understood TTT family specific for C4-dicarboxylate uptake and present the structure of the cognate ligand-bound periplasmic SBP, which has a particularly high affinity for malate. Our results expand the diversity of C4-dicarboxylate transport mechanisms known in bacteria and provide an interesting parallel to the TRAP-type Dct systems. With easily assayable substrates and an SBP structure, the MatBAC transporter might provide a good model system to investigate the molecular biology of the substrate transport and energy-coupling mechanisms of the TTT family.

Materials and Methods

Strains and culture conditions

R. palustris CGA009 was used in this study [43]. PYE was used as a rich growth medium, containing 5 g/L peptone, 5 g/L yeast extract and 5 g/L succinate. RCV medium [44] with 10 mM carbon substrate added was used as the minimal media for growth studies. Growth in liquid media was performed anaerobically at 30 °C, with two 9-W warm white LED lights positioned 20 cm from the culture. Growth on solid media was performed aerobically in the dark. *E. coli* strains were grown aerobically at 37 °C. When used, concentrations of antibiotics for *R. palustris* and *E. coli* were as follows, respectively: chloramphenicol 20 and 34 μg/mL, carbenicillin 100 and 50 μg/mL, and gentamycin 100 and 20 μg/mL.

Protein overexpression and purification

R. palustris CGA009 genomic DNA was extracted using the "GenElute™ Bacterial Genome DNA" kit (Sigma). *matC* (without the N-terminal signal) was amplified by PCR with Accuzyme, using the primers shown in Table 2. The amplified DNA was cloned in pET21a (Novagen), at the NheI-XhoI sites, resulting in a C-terminal His_{6x} tag. The resulting plasmid was transformed into *E. coli* DH5α and subsequently into the *E. coli* BL21(DE3) expression strain. Sequencing of the cloned *matC* gene revealed two amino acid differences when compared with the CGA0009 sequence deposited in the Uniprot database, K134E and K306E (numberings relating to our construct). These are in surface regions of the protein that do not affect ligand binding or the overall structure. Overexpression was performed by growth to OD_{600} 0.6 under carbenicillin selection and subsequent induction with 1 mM IPTG at 37 °C for 3 h. Cells were then harvested by centrifugation (16,000*g*, 10 min), resuspended in 20 mL of binding buffer [20 mM sodium phosphate buffer (pH 7.4), 500 mM sodium chloride, 20 mM imidazole] and lysed by sonication (MSE soniprep 5 × 20 s at 16-μm amplitude with cooling by ice). The resulting cell-free extracts were fractionated using an AKTA system with a 5-mL HisTrapTM HP crude column (GE Healthcare, UK), with the recombinant protein eluted using a 0-to 500-mM imidazole gradient [elution buffer; 20 mM sodium phosphate buffer (pH 7.4), 500 mM sodium chloride, 500 mM imidazole]. Further purification was performed by size exclusion chromatography using a 24-mL 1.6 × 60-cm HiLoadSuperdex 200 column equilibrated with 0.5 M NaCl/50 mM Tris (pH 8.0)/1 mM malate at 1.5 mL/min flow rate in an AKTA system. A calibration curve was generated using Ferritin (440 kDa), aldolase (150 kDa), ovalbumin

Table 2. Primers used in this study

Gene (locus tag)		Sequence 5′–3′	Site
Overexpression			
matC (RPA3494)	Forward	ATAGCTAGCGAGCCGGACCGGTT	NheI
	Reverse	ATATCTCGAGGGGCGTTGTGCCCT	XhoI
RT-PCR			
matC (RPA3494)	Forward	GGCCAGCCGATCGAAATC	
	Reverse	GGCGTGAAGTCCTTGTCA	
rpoD (RPA1288)	Forward	CGACTTCCTGCGCAACTATC	
	Reverse	GGTTGGTGTACTTCTTGGCG	
Deletion			
tttBA1 (RPA2321/20)	Upstream forward (UF1)	GCGTCTAGAACCAGACCACCG	XbaI
	Upstream reverse (UR1)	AAGGCGACCCTGCGCCGAACTGACAT	
	Downstream forward (DF1)	CGGCGCAGG GTCGCCTTCCACGAGGAC	
	Downstream reverse (DR1)	ATAGGATCCTAAGGCACTTCCGCCACC	BamHI
	Deletion check upstream (UC1)	TTCTTCTCTCTTGTTGCACGC	
	Deletion check downstream (DC1)	CGCTGAGATGGCACAGC	
matBA (RPA3496/95)	Upstream forward (UF2)	CCATAGGATCCTCAATCACTGGCTGACCGAG	BamHI
	Upstream reverse (UR2)	CTCGGACTC CGCCTCGTCCATCGGT	
	Downstream forward (DF2)	GACGAGGCGGAGTCCGAGGGGTAATTCCAGC	
	Downstream reverse (DR2)	CCCATATCTAGATGAAGTCCTTGTCAGGCCGAT	XbaI
	Deletion check upstream (UC2)	ACCGGGGCACCTTCG	
	Deletion check downstream (DC2)	CGTTGAGGTTGTCGGTGTG	

Relevant restriction sites used for cloning are underlined.

(44 kDa) and ribonuclease (13.5 kDa), and K_{av} was calculated using the formula K_{av} = (Ve – Vo)/(Vt – Vo).

Differential scanning fluorescence assay

Proteins were screened against a ligand library composed of 84 compounds of various classes, listed by Rosa *et al*. [25]. The screens were performed in 50-μL volumes arrayed on 96-well plates, each reaction composed of 5 μM protein, 1× SYPRO orange dye (Invitrogen), 60 μM ligand and TF buffer [50 mM Tris–HCl (pH 7.4) plus 0.1 M NaCl]. Experiments were performed in an Mx3005P RT-PCR machine (Stratagene), according to the method described by Giuliani *et al*. [45]. Any ligand inducing a thermal shift higher than 2 °C was further investigated by fluorescence spectroscopy.

Fluorescence spectroscopy

Intrinsic tryptophan fluorescence was measured using a Cary Eclipse fluorimeter (Varian Ltd., UK) in a 3-mL final volume containing 0.2 μM of protein in TF buffer [Tris 50 mM (pH 7.4), NaCl 0.1 M]. Excitation was at 280 nm with 5-nm slit width, and scans were performed collecting emission data from 300 to 400 nm with 20-nm slit width. Titrations were performed under the same conditions, but with a fixed emission wavelength of 335 nm. Three technical replicates were used to estimate the K_d, by fitting to the quadratic equation for tight binding as previously described [46].

RT-PCR

R. palustris cultures were grown in triplicates photoheterotrophically in RCV minimal media, with 10 mM of the required carbon source (pyruvate, DL-malate, succinate, fumarate) to OD_{660} 0.4. Cells were harvested and RNA was extracted as described by Guccione *et al*. [47], and diluted to a final concentration of 20 ng/μL. Gene-specific primers were designed using primer3 software [48], aiming to amplify a 100-to 300-bp fragment within the middle of the gene of interest and with a ~58 °C melting temperature. Primers used for *matC* and the control gene *rpoD* are shown in Table 2. Reactions were carried out in a 25-μL volume in a MicroAmp® 96-well optical reaction plate (ABI prism) using the Brilliant III Ultra-fast SYBR Green RT-PCR kit (Agilent), according to the manufacturer's instructions. Each RNA reaction was done in triplicate; reactions using genomic DNA for the standard curve were done in duplicate. PCR amplification was carried out in a Stratagene MX3005p thermal cycler (Agilent) according to the manufacturer's instructions. Data were collected with the associated MxPRO QPCR software (Agilent). A standard curve for each gene was generated using a series of *R. palustris* genomic DNA dilutions. Gene expression between cultures was calculated as relative to *RpoD* expression. The data were analyzed as described previously [49].

Construction of unmarked deletion mutants in *R. palustris*

Cassettes for gene deletion of *tttBA1* and *matBA* in *R. palustris* were generated by PCR with the primers shown in Supplementary Fig. 1 and Table 2, amplifying 500 bp of DNA immediately upstream of the target genes (UF1-UR1 and UF2-UR2) and 500 bp immediately downstream (DF1-DR1 and DF2-DR2). An overlapping PCR [50] was performed to ligate both fragments and the resulting products were cloned into the suicide vector pJQ200ks+ [50] to form pTTTBA and pMATBA, which were separately transformed into *E. coli* DH5α and subsequently into the conjugation strain *E. coli* S-17. A double deletion mutant in *R. palustris* was generated according to Quandt and Hynes [50] by first conjugating with *E. coli* S-17 (pTTTBA), with transconjugants selected on gentamycin containing plates for the recombination of the plasmid into the genome. Individual transconjugants were stabbed on RCV plates with and without gentamycin plus 10% sucrose. Those colonies unable to grow with gentamycin but able to grow in the presence of sucrose were screened by PCR using flanking primers (UC1–DC1 and UC2–DC2; Table 2), designed to amplify from outside the cloned regions (see Supplementary Fig. 1), and sequenced (GATC Biotech) to confirm deletion. One correct corresponding colony was then grown in liquid media, the cells were conjugated with *E. coli* S17–1 (pMATBA), and the selection and screening procedure was repeated. The primers used for deletion of RPA2320–21 (*tttBA1*) and RPA3495–96 (*matBA*) are listed in Table 2.

Protein crystallography

Protein was concentrated using a Vivaspin column (GE Healthcare) to 10 mg/mL in TF Buffer [Tris 50 mM (pH 7.4) NaCl 0.1 M]. A range of crystallization conditions were tested using commercial screens (Molecular Dimensions) in sitting drop experiments (200 nL of protein and 200 nL of a crystallization screen reagent) with the use of a Matrix Hydra II Plus One crystallization robot and drops were left for incubation at 17 °C against 50 μL reservoirs of the corresponding crystallization screen reagent. When necessary, optimizations of the conditions for crystal growth were performed in hanging drop experiments, mixing 3 μL of protein with 3 μL of crystallization reagents. Ultimately, MatC was crystalized in Tris 0.1 M (pH 8.5), $MgCl_2$ 0.2 M and PEG 8000 20% (w/v). Crystals were flash cooled in liquid nitrogen after immersion in a solution of 15% glycerol (v/v) added to the mother liquor.

Data collection and structure determination

Data were collected at the Diamond Light Source (UK) on Beamline station I02. Data processing was done with XDS and merging with XSCALE [51]. Overall, the data were 100% complete to 3 Å (with an $I/\mathrm{sig}I > 2$ for 90% of these) and 90% complete to 2.5 Å (Supplementary Fig. 3). Molecular replacement was performed with PHASER software [52], part of the Collaborative Computational Project, Number 4 (CCP4) software suite [53], using AdpC as a model [25]. The generated maps were analyzed using COOT [54], and models were refined using REFMAC5 [55] software. Processing and refinement statistics are shown in Table 1. After the addition of water molecules, validation was performed with COOT and MOLPROBITY [56]. The structure factors and coordinates can be accessed in the PDB with the accession code 6HKE. Figures were generated using Pymol (The PyMOL Molecular Graphics System, Version 1.8 Schrödinger, LLC) and Ligplot+ [57].

Accession Number

PDB ID: 6HKE

Acknowledgment

The present work was accomplished with funding from Brazilian funding agency CNPQ (National Council for Scientific and Technological Development) through a PhD studentship in the remit of "Science Without Borders" program to L.T.R. (248597/2013-2). May this manuscript reinforce the importance of prioritizing investment in science and research by the Brazilian government.

Author Contributions: L.T.R. designed and executed most of the experiments, analyzed the results and co-wrote the paper. J.B.R. and S.R.D. collected protein crystal diffraction data and built the protein structure model. J.B.R. also edited the paper. D.J.K. conceived the idea for the project, helped to design the experiments, co-wrote and edited the paper and provided supervisory support.

Conflict of Interest Statement: The authors declare that they have no conflicts of interest in connection with the content of this article.

Appendix A. Supplementary data

Supplementary data to this article can be found online at https://doi.org/10.1016/j.jmb.2018.11.016.

Received 24 September 2018;
Received in revised form 14 November 2018;
Accepted 14 November 2018
Available online 22 November 2018

Keywords:
malate;
substrate binding-protein;
secondary transporter;
periplasm;
tryptophan fluorescence

Abbreviations used:
ABC, ATP-binding cassette; SBP, solute binding protein; TM, transmembrane; TRAP transporter, tripartite ATP-independent periplasmic transporter; TTT, tripartite tricarboxylate transporter; RT-PCR, reverse transcription–polymerase chain reaction.

References

[1] G. Unden, A. Strecker, A. Kleefeld, O. Kim, C4-dicarboxylate utilization in aerobic and anaerobic growth, EcoSal Plus 2016 (2016) https://doi.org/10.1128/ecosalplus.ESP-0021-2015.
[2] M.G. Gänzle, Lactic metabolism revisited: metabolism of lactic acid bacteria in food fermentations and food spoilage, Curr. Opin. Food Sci. 2 (2015) 106–117.
[3] J. Ogawa, C.-L. Soong, M. Ito, S. Shimizu, Enzymatic production of pyruvate from fumarate—an application of microbial cyclic-imide-transforming pathway, J. Mol. Catal. B Enzym. 11 (2001) 355–359.
[4] F.W. Larimer, P. Chain, L. Hauser, J. Lamerdin, S. Malfatti, L. Do, et al., Complete genome sequence of the metabolically versatile photosynthetic bacterium *Rhodopseudomonas palustris*, Nat. Biotechnol. 22 (2004) 55–61.
[5] P. Poole, D. Allaway, Carbon and nitrogen metabolism in *Rhizobium*, Adv. Microb. Physiol. 43 (2000) 117–163.
[6] F. Rojo, Carbon catabolite repression in *Pseudomonas*: optimizing metabolic versatility and interactions with the environment, FEMS Microbiol. Rev. 34 (2010) 658–684.
[7] M.J. Mitsch, G.C. Dicenzo, A. Cowie, T.M. Finan, Succinate transport is not essential for symbiotic nitrogen fixation by *Sinorhizobium meliloti* or *Rhizobium leguminosarum*, Appl. Environ. Microbiol. 84 (2018) e01561-17.
[8] M.H. Saier Jr., V.S. Reddy, B.V. Tsu, M.S. Ahmed, C. Li, G. Moreno-Hagelsieb, The Transporter Classification Database (TCDB): recent advances, Nucleic Acids Res. 44 (2016) D372–D379.
[9] S.N. Yurgel, M.L. Kahn, Dicarboxylate transport by rhizobia, FEMS Microbiol. Rev. 28 (2004) 489–501.
[10] I.G. Janausch, E. Zientz, Q.H. Tran, A. Kröger, G. Unden, C4-dicarboxylate carriers and sensors in bacteria, Biochim. Biophys. Acta Bioenerg. 1553 (2002) 39–56.
[11] E. Holger, W. Brita, K. Reinhard, Na+-dependent succinate uptake in *Corynebacterium glutamicum*, FEMS Microbiol. Lett. 77 (1991) 61–66.
[12] J. Jeong, S. Suh, C. Guan, Y.F. Tsay, N. Moran, C.J. Oh, et al., A nodule-specific dicarboxylate transporter from alder is a member of the peptide transporter family, Plant Physiol. 134 (2004) 969–978.

[13] P. Golby, D.J. Kelly, J.R. Guest, S.C. Andrews, Topological analysis of DcuA, an anaerobic C4-dicarboxylate transporter of *Escherichia coli*, J. Bacteriol. 180 (1998) 4821–4827.
[14] H. Teramoto, T. Shirai, M. Inui, H. Yukawa, Identification of a gene encoding a transporter essential for utilization of C4 dicarboxylates in *Corynebacterium glutamicum*, Appl. Environ. Microbiol. 74 (2008) 5290–5296.
[15] J.-W. Youn, E. Jolkver, R. Krämer, K. Marin, V.F. Wendisch, Identification and characterization of the dicarboxylate uptake system DccT in *Corynebacterium glutamicum*, J. Bacteriol. 190 (2008) 6458–6466.
[16] C. Mulligan, G.A. Fitzgerald, D.-N. Wang, J.A. Mindell, Functional characterization of a Na^+-dependent dicarboxylate transporter from *Vibrio cholerae*, J. Gen. Physiol. 143 (2014) 745–759.
[17] C. Mulligan, C. Fenollar-Ferrer, G.A. Fitzgerald, A. Vergara-Jaque, D. Kaufmann, Y. Li, et al., The bacterial dicarboxylate transporter VcINDY uses a two-domain elevator-type mechanism, Nat. Struct. Mol. Biol. 23 (2016) 256–263.
[18] B.P. Krom, J.B. Warner, W.N. Konings, J.S. Lolkema, Transporters involved in uptake of di- and tricarboxylates in *Bacillus subtilis*, Antonie Van Leeuwenhoek 84 (2003) 69–80.
[19] L.T. Rosa, M.E. Bianconi, G.H. Thomas, D.J. Kelly, Tripartite ATP-independent periplasmic (TRAP) transporters and tripartite tricarboxylate transporters (TTT): from uptake to pathogenicity, Front. Cell. Infect. Microbiol. 8 (2018) 33.
[20] D.J. Kelly, G.H. Thomas, The tripartite ATP-independent periplasmic (TRAP) transporters of bacteria and archaea, FEMS Microbiol. Rev. 25 (2001) 405–424.
[21] M.W. Vetting, N. Al-Obaidi, S. Zhao, B. San Francisco, J. Kim, D.J. Wichelecki, et al., Experimental strategies for functional annotation and metabolism discovery: targeted screening of solute binding proteins and unbiased panning of metabolomes, Biochemistry 54 (2015) 909–931.
[22] C. Mulligan, E.R. Geertsma, E. Severi, D.J. Kelly, B. Poolman, G.H. Thomas, The substrate-binding protein imposes directionality on an electrochemical sodium gradient-driven TRAP transporter, Proc. Natl. Acad. Sci. U. S. A. 106 (2009) 1778–1783.
[23] G.D. Sweet, J.M. Somers, W.W. Kay, Purification and properties of a citrate-binding transport component, the C protein of *Salmonella typhimurium*, Can. J. Biochem. 57 (1979) 710–715.
[24] L.T. Rosa, V. Springthorpe, M.E. Bianconi, G.H. Thomas, D.J. Kelly, Massive over-representation of solute-binding proteins (SBPs) from the tripartite tricarboxylate transporter (TTT) family in the genome of the alpha-proteobacterium *Rhodoplanes sp.* Z2-YC6860, Microb. Genom. 4 (2018) https://doi.org/10.1099/mgen.0.000176.
[25] L.T. Rosa, S.R. Dix, J.B. Rafferty, D.J. Kelly, Structural basis for high-affinity adipate binding to AdpC (RPA4515), an orphan periplasmic-binding protein from the tripartite tricarboxylate transporter (TTT) family in *Rhodopseudomonas palustris*, FEBS J. 284 (2017) 4262–4277.
[26] G.D. Sweet, C.M. Kay, W.W. Kay, Tricarboxylate-binding proteins of *Salmonella typhimurium*. Purification, crystallization, and physical properties, J. Biol. Chem. 259 (1984) 1586–1592.
[27] M. Brocker, S. Schaffer, C. Mack, M. Bott, Citrate utilization by *Corynebacterium glutamicum* is controlled by the CitAB two-component system through positive regulation of the citrate transport genes *citH* and *tctCBA*, J. Bacteriol. 191 (2009) 3869–3880.
[28] R.A. Batista-Garcia, A. Sanchez-Reyes, C. Millan-Pacheco, V.M. Gonzalez-Zuniga, S. Juarez, J.L. Folch-Mallol, et al., A novel TctA citrate transporter from an activated sludge metagenome: structural and mechanistic predictions for the TTT family, Proteins 82 (2014) 1756–1764.
[29] J. Herrou, C. Bompard, R. Antoine, A. Leroy, P. Rucktooa, D. Hot, et al., Structure-based mechanism of ligand binding for periplasmic solute-binding protein of the Bug family, J. Mol. Biol. 373 (2007) 954–964.
[30] S. Gonin, P. Arnoux, B. Pierru, J. Lavergne, B. Alonso, M. Sabaty, et al., Crystal structures of an extracytoplasmic solute receptor from a TRAP transporter in its open and closed forms reveal a helix-swapped dimer requiring a cation for alpha-keto acid binding, BMC Struct. Biol. 7 (2007) 11.
[31] N. Akiyama, K. Takeda, K. Miki, Crystal structure of a periplasmic substrate-binding protein in complex with calcium lactate, J. Mol. Biol. 392 (2009) 559–565.
[32] M.J. Cuneo, A. Changela, A.E. Miklos, L.S. Beese, J.K. Krueger, H.W. Hellinga, Structural analysis of a periplasmic binding protein in the tripartite ATP-independent transporter family reveals a tetrameric assembly that may have a role in ligand transport, J. Biol. Chem. 283 (2008) 32812–32820.
[33] K. Fukami-Kobayashi, Y. Tateno, K. Nishikawa, Domain dislocation: a change of core structure in periplasmic binding proteins in their evolutionary history, J. Mol. Biol. 286 (1999) 279–290.
[34] G.H. Scheepers, A. Lycklama, J.A. Nijeholt, B. Poolman, An updated structural classification of substrate-binding proteins, FEBS Lett. 590 (2016) 4393–4401.
[35] I. Huvent, H. Belrhali, R. Antoine, C. Bompard, C. Locht, F. Jacob-Dubuisson, et al., Crystal structure of *Bordetella pertussis* BugD solute receptor unveils the basis of ligand binding in a new family of periplasmic binding proteins, J. Mol. Biol. 356 (2006) 1014–1026.
[36] I. Huvent, H. Belrhali, R. Antoine, C. Bompard, C. Locht, F. Jacob-Dubuisson, et al., Structural analysis of *Bordetella pertussis* BugE solute receptor in a bound conformation, Acta Crystallogr. D Biol. Crystallogr. 62 (2006) 1375–1381.
[37] M. Hosaka, N. Kamimura, S. Toribami, K. Mori, D. Kasai, M. Fukuda, et al., Novel tripartite aromatic acid transporter essential for terephthalate uptake in *Comamonas* sp. strain E6, Appl. Environ. Microbiol. 79 (2013) 6148–6155.
[38] K. Denger, A.M. Cook, Racemase activity effected by two dehydrogenases in sulfolactate degradation by *Chromohalobacter salexigens:* purification of (*S*)-sulfolactate dehydrogenase, Microbiology (UK) 156 (2010) 967–974.
[39] A.M. Pudlik, J.S. Lolkema, Substrate specificity of the citrate transporter CitP of *Lactococcus lactis*, J. Bacteriol. 194 (2012) 3627–3635.
[40] C.B. van Niel, The culture, general physiology, morphology, and classification of the non-sulfur purple and brown bacteria, Bacteriol. Rev. 8 (1944) 1–118.
[41] R.C. Salmon, M.J. Cliff, J.B. Rafferty, D.J. Kelly, The CouPSTU and TarPQM transporters in *Rhodopseudomonas palustris*: redundant, promiscuous uptake systems for lignin-derived aromatic substrates, PLoS One 8 (2013), e59844.
[42] D. Sengupta, R.N. Behera, J.C. Smith, G.M. Ullmann, The α helix dipole: screened out? Structure 13 (2005) 849–855.
[43] M.-K. Kim, C.S. Harwood, Regulation of benzoate-CoA ligase in *Rhodopseudomonas palustris*, FEMS Microbiol. Lett. 83 (1991) 199–203.
[44] J.T. Beatty, H. Gest, Biosynthetic and bioenergetic functions of citric acid cycle reactions in *Rhodopseudomonas capsulata*, J. Bacteriol. 148 (1981) 584–593.

[45] S.E. Giuliani, A.M. Frank, D.M. Corgliano, C. Seifert, L. Hauser, F.R. Collart, Environment sensing and response mediated by ABC transporters, BMC Genomics 12 (Suppl. 1) (2011) S8.
[46] J.P. Smart, M.J. Cliff, D.J. Kelly, A role for tungsten in the biology of *Campylobacter jejuni*: tungstate stimulates formate dehydrogenase activity and is transported via an ultra-high affinity ABC system distinct from the molybdate transporter, Mol. Microbiol. 74 (2009) 742–757.
[47] E. Guccione, M. Del Rocio Leon-Kempis, B.M. Pearson, E. Hitchin, F. Mulholland, P.M. Van Diemen, et al., Amino acid-dependent growth of *Campylobacter jejuni*: key roles for aspartase (AspA) under microaerobic and oxygen-limited conditions and identification of AspB (Cj0762), essential for growth on glutamate, Mol. Microbiol. 69 (2008) 77–93.
[48] A. Untergasser, I. Cutcutache, T. Koressaar, J. Ye, B.C. Faircloth, M. Remm, et al., Primer3—new capabilities and interfaces, Nucleic Acids Res. 40 (2012) (e115-e).
[49] R. Higuchi, B. Krummel, R.K. Saiki, A general method of in vitro preparation and specific mutagenesis of DNA fragments: study of protein and DNA interactions, Nucleic Acids Res. 16 (1988) 7351–7367.
[50] J. Quandt, M.F. Hynes, Versatile suicide vectors which allow direct selection for gene replacement in gram-negative bacteria, Gene 127 (1993) 15–21.
[51] W. Kabsch, XDS, Acta Crystallogr. D Biol. Crystallogr. 66 (2010) 125–132.
[52] A.J. McCoy, R.W. Grosse-Kunstleve, P.D. Adams, M.D. Winn, L.C. Storoni, R.J. Read, Phaser crystallographic software, J. Appl. Crystallogr. 40 (2007) 658–674.
[53] M.D. Winn, C.C. Ballard, K.D. Cowtan, E.J. Dodson, P. Emsley, P.R. Evans, et al., Overview of the CCP4 suite and current developments, Acta Crystallogr. D Biol. Crystallogr. 67 (2011) 235–242.
[54] P. Emsley, K. Cowtan, Coot: model-building tools for molecular graphics, Acta Crystallogr. D Biol. Crystallogr. 60 (2004) 2126–2132.
[55] G.N. Murshudov, A.A. Vagin, E.J. Dodson, Refinement of macromolecular structures by the maximum-likelihood method, Acta Crystallogr. D Biol. Crystallogr. 53 (1997) 240–255.
[56] V.B. Chen, W.B. Arendall, J.J. Headd, D.A. Keedy, R.M. Immormino, G.J. Kapral, et al., MolProbity: all-atom structure validation for macromolecular crystallography, Acta Crystallogr. D Biol. Crystallogr. 66 (2010) 12–21.
[57] R.A. Laskowski, M.B. Swindells, LigPlot+: multiple ligand–protein interaction diagrams for drug discovery, J. Chem. Inf. Model. 51 (2011) 2778–2786.